

Supporting Information

Controlling Crystallographic Orientation in h-WO₃ Films to Maximize Photoelectrochemical Water Splitting

Wenhao He^a, Wenzhang Li^a, Jianye Liu^a, Ge Lou^a, Chenyu Zhang^a,

Yang Liu^{a, *}, Jie Li^{a, *}

^a School of Chemistry and Chemical Engineering, Central South

University, Changsha, 410083, China

Corresponding author: yangliu_csu@csu.edu.cn; lijieliu@csu.edu.cn

Experimental section

1.1 Materials

Ammonium metatungstate hydrate (AMT: $(\text{NH}_4)_6\text{H}_2\text{W}_{12}\text{O}_{40}\cdot x\text{H}_2\text{O}$), hydrochloric acid (HCl, 12M), hydrogen peroxide solution (H_2O_2 , 30wt%), oxalic acid dihydrate ($\text{C}_2\text{H}_2\text{O}_4\cdot 2\text{H}_2\text{O}$, 99.5%), tungstic acid (H_2WO_4), urea (H_2NCONH_2 , 99%), acetonitrile (CH_3CN). Potassium dihydrogen phosphate (KH_2PO_4 , 99.5%), and dipotassium hydrogen phosphate trihydrate ($\text{K}_2\text{HPO}_4\cdot 3\text{H}_2\text{O}$, 99%) were obtained from Sinopharm Chemical Reagent Co., Ltd. (Shanghai, China). All chemicals can be suitable for direct use. The water used for the reaction in the laboratory was deionized water.

1.2 Preparation of WO_3 -110 photoanode

The h- WO_3 thin film photoanodes were fabricated directly on FTO glass using a hydrothermal method. Initially, 0.75 g of ammonium metatungstate was dissolved in 75 mL of deionized water, followed by the addition of 3 mL of concentrated hydrochloric acid, and stirred for 10 minutes. Subsequently, 1.5 mL of 30wt% hydrogen peroxide (H_2O_2) was introduced. A piece of cleaned FTO glass ($3\times 4\text{ cm}^2$), with the conductive side facing down, was placed in a 100 mL Teflon reactor filled with the solution. The assembly was then subjected to treatment at 170 °C for 4 hours, allowed to cool naturally, and the film was subsequently rinsed with DI water. The film was dried at room temperature and then further heat-treated in air at 400 °C for 2 hours. The resulting material was denoted as **WO_3 -110**. (Fig. 1a)

1.3 Preparation of WO_3 -200 photoanode

Based on the preparation of WO_3 -110 photoanodes, an additional 1.11105g of oxalic acid was added after stirring 1.5 mL of 30 wt.% H_2O_2 for a period of time to fully dissolve and form a transparent precursor. The following experimental procedures and conditions were the same as those in WO_3 -110. The resulting photoanode after the reaction is called **WO_3 -200** (Fig. 1b).

1.4 Preparation of WO_3 -001 photoanode

WO_3 -001 photoanode was prepared using the solvothermal method. First, 1 g of H_2WO_4 and 0.4 g of polyvinyl alcohol (PVA) were dissolved and dispersed in 12 mL of H_2O_2 to prepare the seed crystal masterbatch. The prepared seed crystal masterbatch

was spin-coated on a conductive glass FTO at a speed of 2000 rpm for 18 s and annealed at 500 °C for 1 h in air. Subsequently, 1 g of H₂WO₄ was added to 28 mL of DI water and 12 mL of H₂O₂ and heated to 95°C to facilitate dissolution and obtain the reaction masterbatch. Finally, 0.1 g of oxalic acid, 0.1 g of urea, 1.25 mL of HCl (12 M), 5.0 mL of DI water, and 10.0 mL of H₂WO₄ masterbatch were added to 62.5 mL of acetonitrile. The resulting solution was transferred to a 100 mL Teflon reactor containing FTO (loaded with a seed layer) and treated at 180 °C for 2 h. After natural cooling, the film was washed several times with DI water, dried at room temperature, and then treated at 400 °C for 2 h in air. This sample was labeled as **WO₃-001 (Fig. 1c)**.

1.5 Characterization and photoelectrochemical performance

The **UV-Vis** optical properties of the samples were analyzed using the TU-1901 dual-beam UV-visible spectrophotometer from Beijing General. The crystallinity and growth orientation of the h-WO₃ photoanodes were determined using an X-ray powder diffractometer (**XRD**, Japan/Ultima IV) with Cu K α radiation (40 kV, 450 mA, λ = 0.1541 nm). **XRD texture** analysis was conducted to investigate the crystal structure, texture orientation, and directionality of the samples using the Smartlab equipment. The elemental composition and valence states of the three types of h-WO₃ surfaces were analyzed using X-ray photoelectron spectroscopy (**XPS**, Thermo Fisher Scientific/NEXSA). The microstructural growth morphology of the thin film photoanodes was observed using a scanning electron microscope (**SEM**, JEOL/JSM-7610FPlus). Transmission electron microscopy (**TEM**) images were captured using a high-resolution transmission electron microscope (JEOL JEM 2100). Spherical aberration electron microscopy tests were carried out using a condenser spherical aberration-corrected transmission electron microscope (**ABF-STEM**, Thermo Scientific, Themis Z). Measurement of steady-state photoluminescence spectra and fluorescence lifetimes using the Edinburgh Steady-State/Transient Fluorescence Spectrometer (**PL**, **FLS1000**). Surface band structure analysis of the samples was conducted using ultraviolet photoelectron spectroscopy (**UPS**, Thermo ESCALAB 250XI).

All samples were analyzed using a three-electrode system at 25 °C in a 0.2 M KPi solution (pH \approx 7). The working electrode consisted of the thin film photoanode, while a Pt electrode served as the counter electrode, and the Ag/AgCl electrode served as the reference electrode. A series of photoelectrochemical tests were performed under AM 1.5G simulated solar light irradiation (light intensity of 100mW cm⁻²), and 0.2 M Na₂SO₃ was added as a hole sacrificial agent. The photochemical tests were carried out on the electrochemical workstation IGS1130, while the Electrochemical Impedance Spectroscopy (EIS) and Intensity Modulated Photocurrent Spectroscopy (IMPS) were performed on the Zahner electrochemical workstation.

1.6 Density functional theory (DFT) calculation

The density functional theory (DFT) calculation was performed using Vienna ab initio simulation package (VASP),^{1, 2} and Perdew–Burke–Ernzerhof functional (PBE) with DFT-D3 were considered.³ According to the XRD and TEM results, h-WO₃(110) and h-WO₃(001) were selected. The energy of slabs before and after absorbing NH₄⁺ were calculated. For calculation, the energy cutoff, Gaussian searing, force, total energy were 400 eV, 0.1 eV, 0.02 eV/Å and 5.0×10⁵ eV, and the dipole correction as well as spin polarization were applied.

Supplementary Figures

Table S1 The XRD peak intensity ratios for WO₃-110, WO₃-200 and WO₃-001

	(001)/(110)	(110)/(110)	(200)/(110)	(101)/(110)	(201)/(110)
WO₃-110	0.03	1.00	0.17	0.03	0.04
WO₃-200	0.32	1.00	1.03	0.17	0.35
WO₃-001	7.11	1.00	1.35	1.37	0.72

XRD texture pole figure to determine the crystal structure texture orientation and directionality of h-WO₃

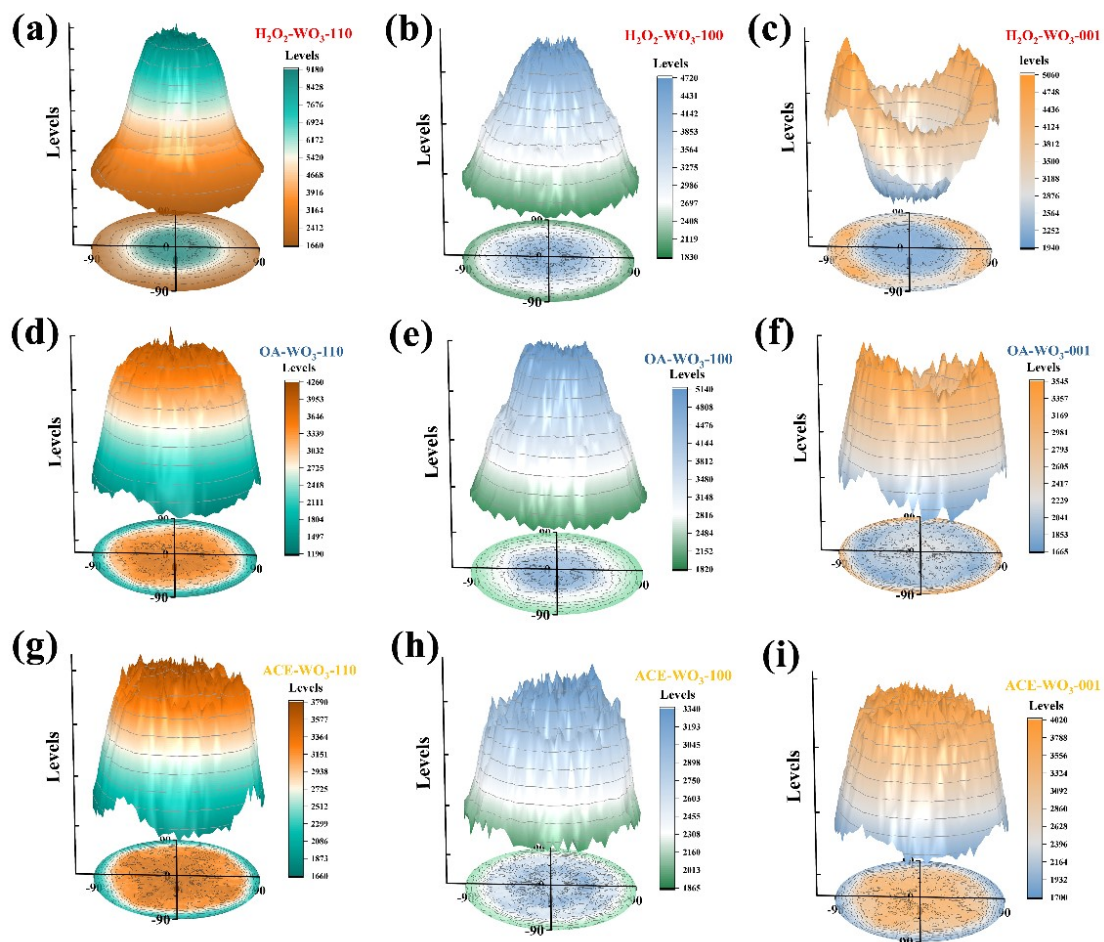


Fig. S1. XRD texture pole figures of h-WO₃ film after calcination: (a)-(c) H₂O₂-WO₃; (d)-(f) OA-WO₃; (g)-(i) ACE-WO₃

In order to distinguish them more clearly, we named the three h-WO₃ of WO₃-110, WO₃-200, and WO₃-001 as H₂O₂-WO₃, OA-WO₃, and ACE-WO₃ respectively to facilitate subsequent testing of their textural compositions. From the XRD results, it can be observed that in addition to the dominant peaks, there are other peaks showing obvious crystal texture characteristics. Since the positions of the three peaks (001), (110), and (200) are close to each other, to prevent interference in the experimental results, we measured the (110), (001), and (100) peaks of these three types of h-WO₃, respectively. Detailed XRD texture pole testing is conducted to further analyze the crystal structure's texture orientation and directionality of the sample. These samples were named "***-WO₃-facets".

TEM; HRTEM; and SAED plots for each photoanode

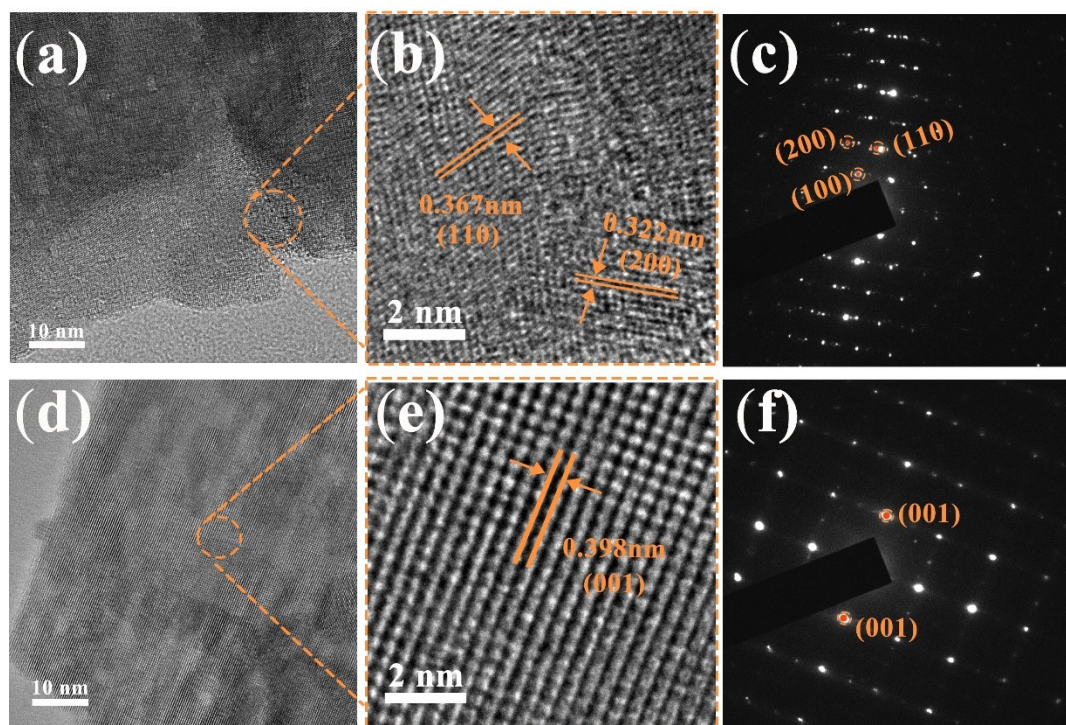


Fig. S2. TEM images of (a)WO₃-200, (d) WO₃-001; HRTEM images of (b)WO₃-200, (e) WO₃-001; SAED images of (c) WO₃-200, (f) WO₃-001.

X-ray diffraction testing (XRD) and XRD texture (pole figure) testing

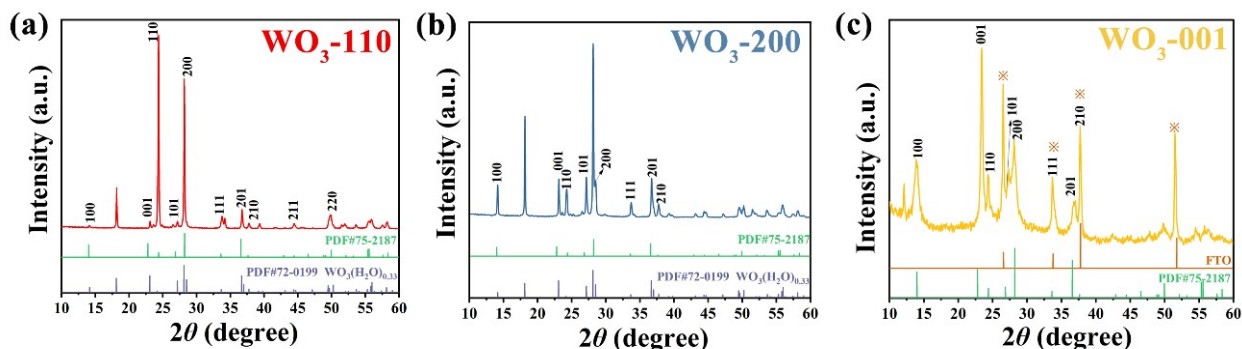


Fig. S3. XRD patterns of h-WO₃ films before calcination: (a) WO₃-110; (b) WO₃-200; (c) WO₃-001 (c) WO₃-001

The samples were characterized by X-ray diffraction (XRD) to determine their crystal structure and crystal facet orientation. **In Fig. S3a-c**, the XRD patterns clearly show that the films obtained by hydrothermal growth exhibit different crystal plane growth orientations. Prior to calcination, most of its diffraction peaks are consistent with the standard profiles of h-WO₃ (JCPDS no. 75-2187)⁴ and WO₃·0.33 H₂O (JCPDS no. 72-0199)⁵. The WO₃-110, WO₃-200, and WO₃-001 samples display strong exposed surfaces corresponding to (110), (200), and (001) facets, respectively. Some of the characteristic peaks in **Fig. S3c** that correspond to the characteristic peaks of SnO₂ in the standard map (JCPDS no. 46-1088) can be attributed to the FTO glass used in our experiments.

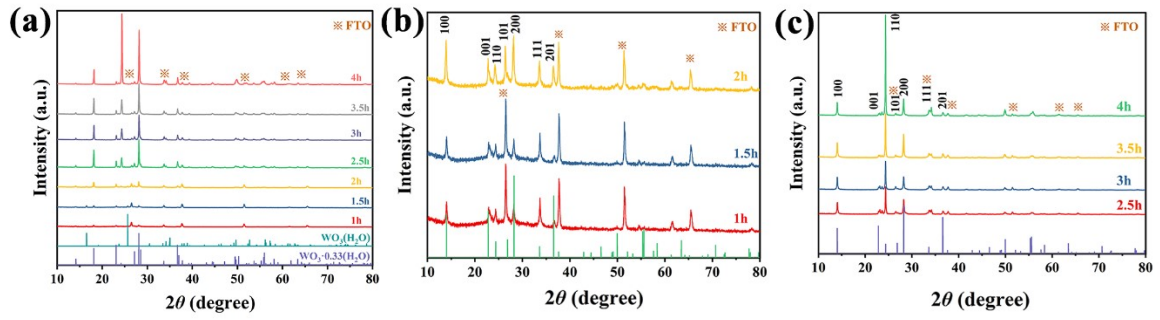
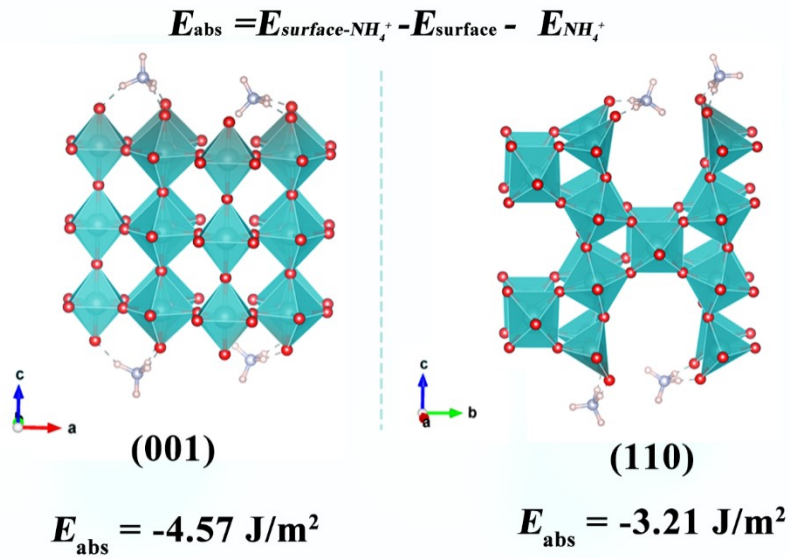


Fig. S4. XRD patterns of (a) WO₃-110 post-calcination at different reaction durations; (b) WO₃-110 during the first two hours of reaction, and (c) WO₃-110 after two hours of reaction.

NH₄⁺ surface adsorption energy calculation :



Ultraviolet-visible (UV-Vis)

The diffuse reflectance spectra were converted to the corresponding UV-vis absorption spectra using **Equation (S1)**. The Tauc diagram was plotted using **Formula (S2)**. The energy gaps of WO₃-110, WO₃-200, and WO₃-001 were determined by plotting tangent lines.

$$\alpha = \lg\left(\frac{100}{R}\right) \quad (\text{S1})$$

$$(\alpha h\nu)^{\frac{1}{2}} = A(h\nu - E_g) \quad (\text{S2})$$

α represents absorbance, $h\nu$ denotes photon energy, A stands for the constant, and E_g signifies the band gap.

Ultraviolet photoelectron spectroscopy (UPS)

To determine the relative band edge positions of h-WO₃ crystals, we utilized ultraviolet photoelectron spectroscopy (UPS) to analyze the surface band structure of the samples. Based on UPS data, along with **equation S3**, we calculated the work function (Φ) of each sample, while **equation S4** enabled us to determine the position of each valence band edge. Further analysis of the band gap enabled us to clarify the band structure in greater detail.

$$\Phi = 21.2 \text{ eV} - E_{\text{Femi}} \quad (\text{S3})$$

$$E_{\text{VB}} = \Phi + E_{\text{cutoff}} \quad (\text{S4})$$

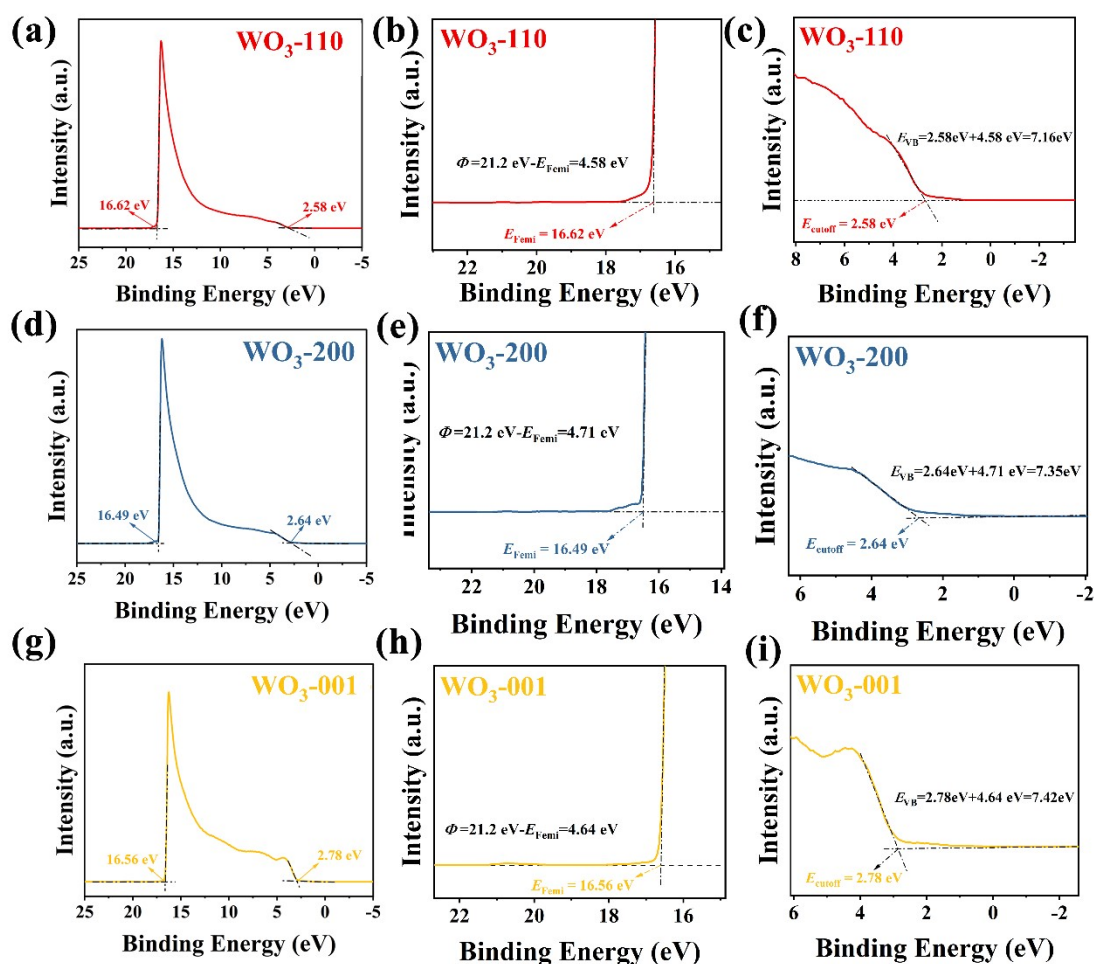


Fig. S5. (a)-(i) UPS spectra of three photoanodes.

photoelectrochemical performance :

All experiments were conducted using a three-electrode setup in a 0.1 M KPi solution (pH \approx 7) at 25°C. The working electrode consisted of a thin-film photoanode, with a Pt sheet serving as the counter electrode, and Ag/AgCl as the reference electrode. Photoelectrochemical assessments were conducted under AM 1.5G simulated solar illumination (light intensity of 100 mW cm⁻²), supplemented with 0.2 M Na₂SO₃ as a hole sacrificial agent. Various photoelectrochemical evaluations of the photoanode were conducted using the IGS1130 electrochemical workstation. Intensity-modulated photocurrent spectroscopy (IMPS) and electrochemical impedance spectroscopy (EIS) were conducted using the Zahner electrochemical workstation in Germany. For IMPS, a direct current (DC) of 50 mA was applied to the light source, with a disturbance current of 5 mA, tested across a frequency range from 1 kHz to 0.1 Hz. EIS analysis was conducted in a 0.1 M KPi solution at 1.23 V vs. RHE, using an amplitude perturbation of 10 mV and a frequency range from 10⁴ Hz to 10⁻¹ Hz.

All electrode potentials were converted to the reversible hydrogen electrode (RHE) reference by applying **Equation S3**.

$$E_{RHE} = E_{Ag/AgCl} + 0.059 * pH + 0.197 \quad (S5)$$

Where E_{RHE} represents the reversible hydrogen electrode, $E_{Ag/AgCl}$ denotes the electrode potential relative to the reference electrode Ag/AgCl, and pH indicates the pH value of the electrolyte solution.

j_{abs} estimate:

Assuming complete conversion of absorbed light into photocurrent, the maximum photocurrent densities for WO₃-110, WO₃-200, and WO₃-001 were calculated using **formula S6**, in conjunction with the UV-visible diffuse reflectance spectra.

$$j_{abs} = q \int \Phi_{\lambda} [1 - \exp(-\alpha_{\lambda}d)] d\lambda \quad (S6)$$

In the formula, q represents the electron charge, λ stands for the wavelength, Φ_{λ} denotes the photon flux, d indicates the photoanode film thickness, and α represents the absorption coefficient. The maximum photocurrent densities of WO₃-110, WO₃-200,

and WO₃-001 were calculated by formula (S6) as follows: **3.36 mA·cm⁻²**, **3.58 mA·cm⁻²**, and **2.17 mA·cm⁻²**, respectively.

η_{sep} and η_{inj} calculation

The carrier separation efficiency (η_{sep}) and carrier injection efficiency (η_{inj}) can be calculated using the following formulas:

$$\eta_{sep} = (j_{KPi + Na_2SO_3}) / (j_{abs}) \dots\dots(S7)$$

$$\eta_{inj} = (j_{KPi}) / (j_{KPi + Na_2SO_3}) \quad (S8)$$

Among them, $j_{KPi + Na_2SO_3}$ represents the photocurrent density measured with 0.2 M Na₂SO₃ as a hole sacrificial agent to a **0.2 M KPi** solution. j_{abs} denotes the theoretical maximum photocurrent density for the three samples, while j_{KPi} represents the photocurrent density measured in a **0.2 M KPi** solution.

Table. S2 The synthesis method and photocurrent density of pure WO₃ in recent years

Material	Method	Electrolyte used	Current density	Reference
h-WO ₃ @110	hydrothermal method	0.2 M KPi (PH=7)	1.86 mA cm ⁻² at 1.23 V vs V _{RHE}	This work
h-WO ₃ nanotree @001@W	hydrothermal method	0.5 M Na ₂ SO ₄	0.07 mA cm ⁻² at 1.23 V vs V _{RHE}	6
h-WO ₃ powder @FTO	spin-coated	0.5 M Na ₂ SO ₄	0.25 μA cm ⁻² at 1.23 V vs V _{RHE}	7
h-WO ₃ nanosphere @FTO	hydrothermal method	0.5 M Na ₂ SO ₄	0.37 mA cm ⁻² at 1.23 V vs V _{RHE}	8
h-WO ₃ @101@FTO	hydrothermal method	0.1 M Na ₂ SO ₄	0.19 mA cm ⁻² at 1.23 V vs V _{RHE}	9
Cr doped h-WO ₃ @001@FTO	hydrothermal method	0.5 M Na ₂ SO ₄	0.024 mA cm ⁻² at 1.23 V vs V _{RHE}	10
h-WO ₃ @200@FTO	dip-coating	0.1 M Na ₂ SO ₄	6 μA cm ⁻² at 0.0 V (vs. SCE)	11
h-WO ₃ @200@FTO	electrophoretic deposition (EPD)	0.5 M Na ₂ SO ₄	0.35 mA cm ⁻² at 1.23 V vs V _{RHE}	12
h-WO ₃ @FTO	hydrothermal method	0.5 M Na ₂ SO ₃ (PH=7.2)	0.44 mA cm ⁻² at 1.23 V vs V _{RHE}	13
h-WO ₃ @ITO	hydrothermal method	0.5 M Na ₂ SO ₄	0.35 μA cm ⁻² at 1.23 V vs V _{RHE}	14
h-WO ₃ @FTO	WO ₃ nanopowders coated	0.5 M Na ₂ SO ₄	0.11 mA cm ⁻² at 0.0 V (vs. SCE)	15
h-WO ₃ @FTO	hydrothermal method	1 M H ₂ SO ₄	0.45 mA cm ⁻² at 0.8 V vs V _{RHE}	16
m-WO ₃	hydrothermal method	0.5 Na ₂ SO ₄	0.5 mA cm ⁻² at 1.23 V vs V _{RHE}	17
m-WO ₃	hydrothermal method	0.5 M Na ₂ SO ₄	0.3 mA cm ⁻² at 1.23 V vs V _{RHE}	18

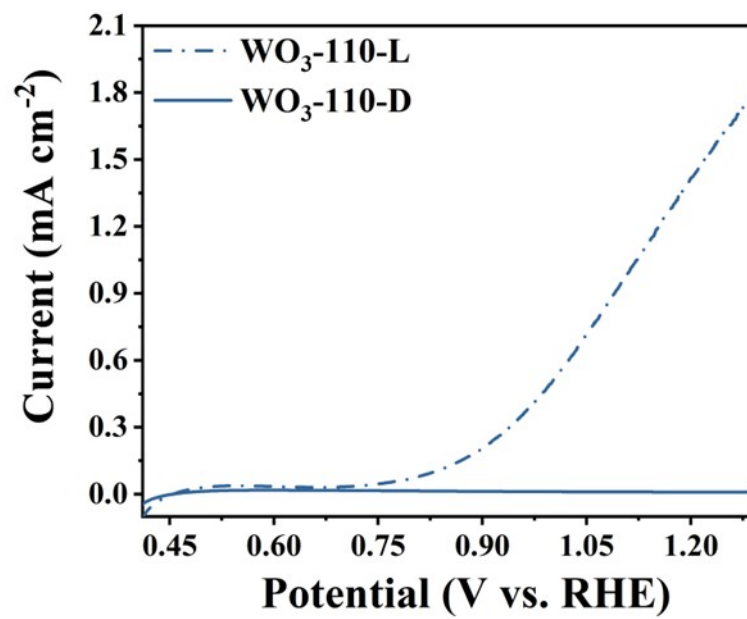


Fig. S6. The LSV Curve of WO₃-110 in the 0.5M Na₂SO₄ solution

Electrochemical Active Surface area (ECSA)

To investigate the impact of surface capacitance on the PEC performance of the three h-WO₃ photoanodes, the CV curves of the three photoanodes in the non-Faraday region at 0.41 - 0.61 V vs. RHE with different sweep rates (20 mV/s to 100 mV/s) were obtained using cyclic voltammetry (**Fig. S7**). A plot of current difference (Δj) versus sweep rate (ν) was obtained by calculating the current difference versus sweep rate at 0.51 V vs. RHE. Since the WO₃ bilayer capacitance C_{dl} is half of the slope of the Δj - ν curve¹⁹, the ECSAs of WO₃-110, WO₃-200, and WO₃-001 can be roughly calculated according to **Eq. (S9)**.

$$ECSA = \frac{C_{dl}}{C_s} \quad (S9)$$

Where C_s represents the capacitance per unit area of the sample, which is typically a constant value within the same electrolyte. C_{dl} denotes the double-layer capacitance of WO₃.

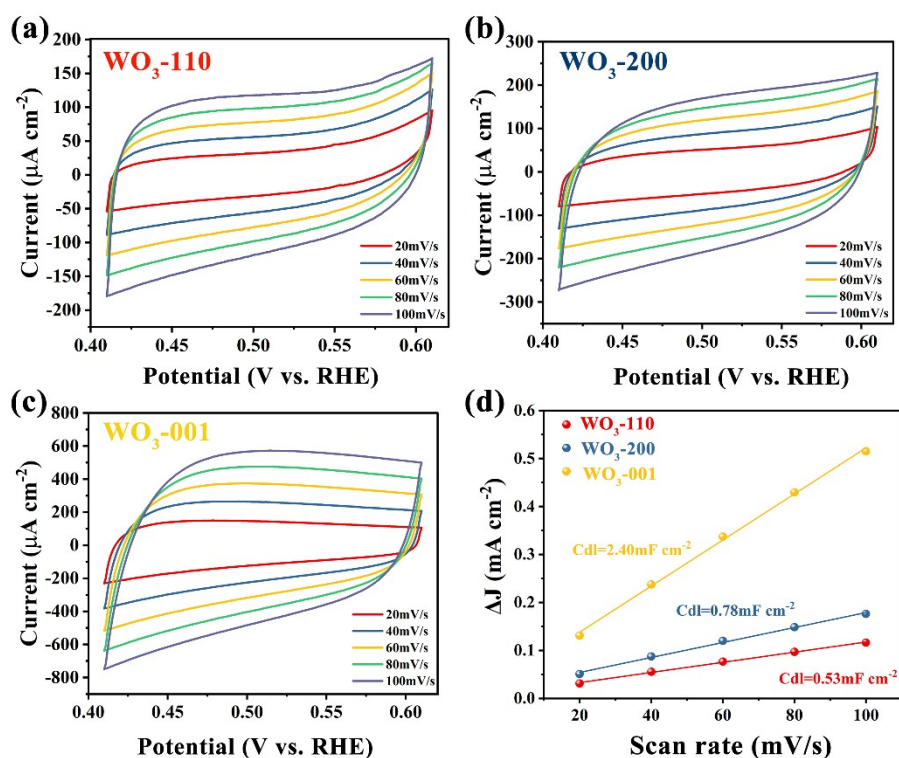


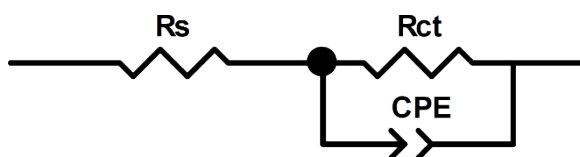
Fig. S7. The cyclic voltammetry results for (a) WO₃-110, (b) WO₃-200, and (c) WO₃-001. (d) the anode-cathode current difference at different scan rates (0.51 V vs. RHE).

Electrochemical Impedance Spectroscopy (EIS)

Table S3. Summary of Parameters from EIS Fitting of WO₃-110, WO₃-200, and WO₃-001 in 0.2M KPi solution

Photoanode	$R_s(\Omega)$	$R_{CT}(\Omega)$	$CPE-T$	$CPE-P$
WO ₃ -110	29.34	374.9	0.000260	0.8421
WO ₃ -200	17.9	1057	0.000465	0.4964
WO ₃ -001	23.94	5316	0.000020	0.9079

Electrochemical impedance fitting equivalent circuit diagram



The electron lifetimes (τ)

The electron lifetimes (τ) of the three photoanodes were calculated using **Eq. (S10)** and the frequency (f) at the lowest point in the plot.

$$\tau = \frac{1}{2\pi f} \quad (\text{S10})$$

Modulated Photocurrent Spectroscopy (IMPS)

The semicircles of all the samples appeared in the fourth quadrant. Among them, the magnified view of WO₃-001 is shown in Fig. S7. According to Eq. (S11) and the frequency (f_{min}) at the lowest point, the electron transfer time (τ_{et}) of the three photoanodes can be found.

$$\tau_{et} = \frac{1}{2\pi f_{min}} \quad (S11)$$

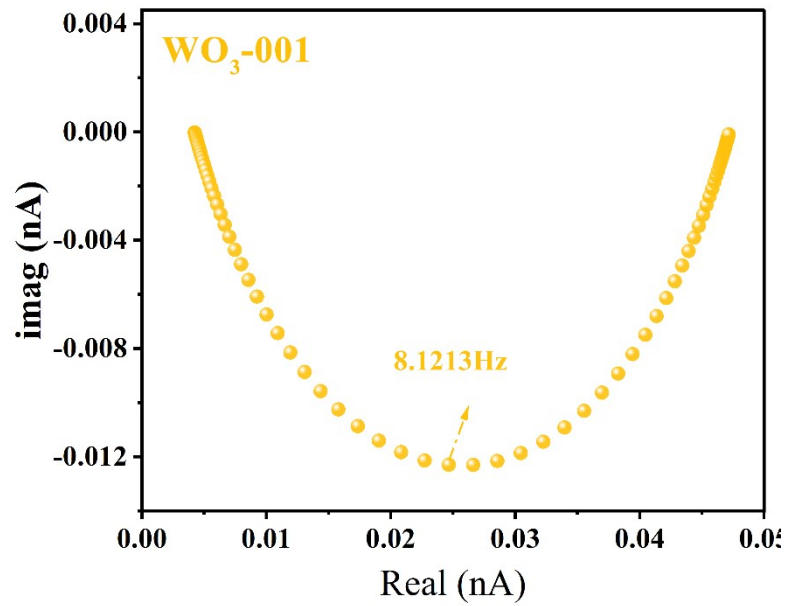


Fig. S8. The magnified plot of IMPS for WO₃-001.

Table S4. Biexponential decay-fitted parameters of time-resolved photoluminescence decay curves for WO₃-110, WO₃-200, and WO₃-001 photoanodes

photoanodes	τ_1/ns	τ_2/ns	τ_3/ns	B ₁ (%)	B ₂ (%)	B ₃ (%)	$\tau_{\text{ave}}/\text{ns}$
WO ₃ -110	1.30	4.96	20.38	14.90	66.41	18.69	12.91
WO ₃ -200	0.85	4.02	15.40	37.57	44.04	18.39	10.37
WO ₃ -001	0.70	3.53	15.16	23.40	52.84	23.76	10.89

Biexponential function fitting was employed to analyze the time-resolved photoluminescence decay curves, and the average recombination lifetime, t_{average} was calculated by the following Equation (S12).

$$t_{\text{average}} = \frac{B_1\tau_1^2 + B_2\tau_2^2 + B_3\tau_3^2}{B_1\tau_1 + B_2\tau_2 + B_3\tau_3} \quad (\text{S12})$$

In the formula, τ_1 , τ_2 and τ_3 are defined as the decay time for the fluorescence intensity, representing the speed of carrier recombination.

Incident Monochromatic Photon-Electron Conversion Efficiency (IPCE)

The Incident Photon-to-Current Efficiency (IPCE) is a critical metric for evaluating the photoelectrochemical performance of electrodes across different wavelengths. It quantifies the efficiency of photon-to-current conversion. The formula for calculating IPCE is given by follows S13:

$$IPCE = (|j_{photo}| * 1240) / (P_{mono} * \lambda) \quad (S13)$$

Where j_{photo} denotes the photocurrent density ($\text{mA}\cdot\text{cm}^{-2}$), P_{mono} signifies the optical power of monochromatic light ($\text{mW}\cdot\text{cm}^{-2}$), and λ represents the wavelength of monochromatic light.

Light Harvesting Efficiency (LHE)

LHE stands for "Light Harvesting Efficiency", which measures how effectively a material absorbs incident light within a specific wavelength range. The value is calculated using Formula S14.

$$LHE = 1 - 10^{-A(\lambda)} \quad (S14)$$

where A represents the absorbance corresponding to the wavelength

Absorbed Photon-to-Current Conversion Efficiency (APCE)

APCE assesses the ability of a photoelectrode to convert absorbed incident light into electrical current. A higher APCE value signifies greater efficiency in photon absorption and current generation by the photoelectrode. APCE is calculated using formula S15

$$APCE = IPCE / LHE \quad (S15)$$

Applied Bias Photon-to-current Efficiency (ABPE)

ABPE quantifies the ratio of solar energy converted to hydrogen energy under specific bias voltage conditions. It is calculated using formula S16.

$$ABPE = (|j_{photo}| * (1.23 - E)) / P_{mono} \quad (S16)$$

where j_{photo} is the photocurrent density when bias voltage E is applied, and P_{mono} is the incident light intensity.

Open-circuit Potential (OCP)

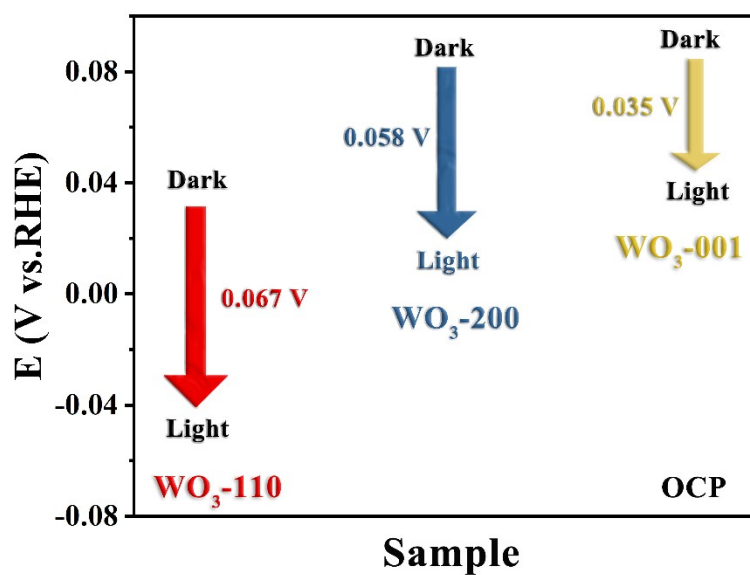


Fig. S9. The open circuit potential (OCP) transient decay profile.

The stability of the photoanode was tested in a 0.1 M KPi solution (i-t).

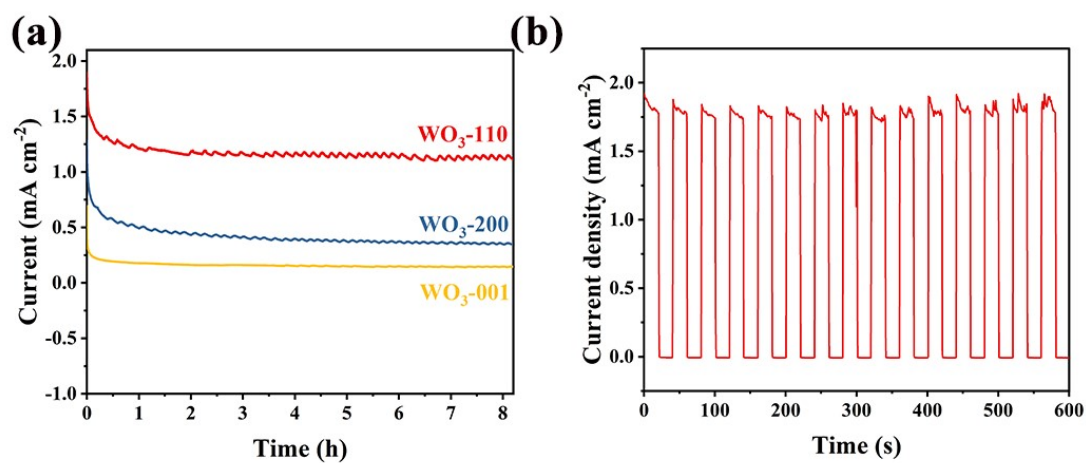


Fig. S10. (a) Current-time (i-t) curves measured in 0.2 M KPi (pH=5) solution. (b) Light chopping graph at 1.23 V vs. RHE i-t test (light 20s, dark 20s)

Quantitative analysis of hydrogen and oxygen production in PEC water splitting.

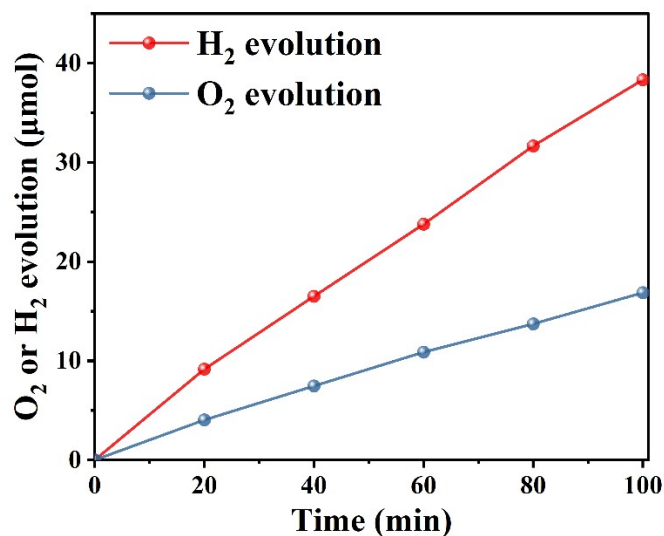


Fig. S11. Quantitative analysis of hydrogen and oxygen production in PEC water splitting.

Table S5. Data organization for the quantitative analysis of hydrogen and oxygen production in photoelectrochemical water splitting

t (s)	Hydrogen production.(μmol)	H ₂ Faradaic efficiency.	Oxygen production.(μmol)	O ₂ Faradaic efficiency.
1200	9.15	98.12	4.04	86.60
2400	16.50	98.29	7.46	88.84
3600	23.77	97.25	10.88	89.01
4800	31.66	99.45	13.73	86.22
6000	38.33	97.83	17.72	90.44

The formula for Faradaic efficiency of products is: (S17)

$$FE = \frac{m \times n \times F}{I \times t} \times 100\% \quad (\text{S17})$$

“m” represents the number of electrons required to produce the product, “n” is the number of moles of the product, “F” is the Faraday constant (96485 C·mol⁻¹), “I” is the average current density, and “t” is the reaction time.

Photoelectrocatalytic Performance of WO₃-110 for Glucose and Glycerol Oxidation: LSV and i-t Analysis

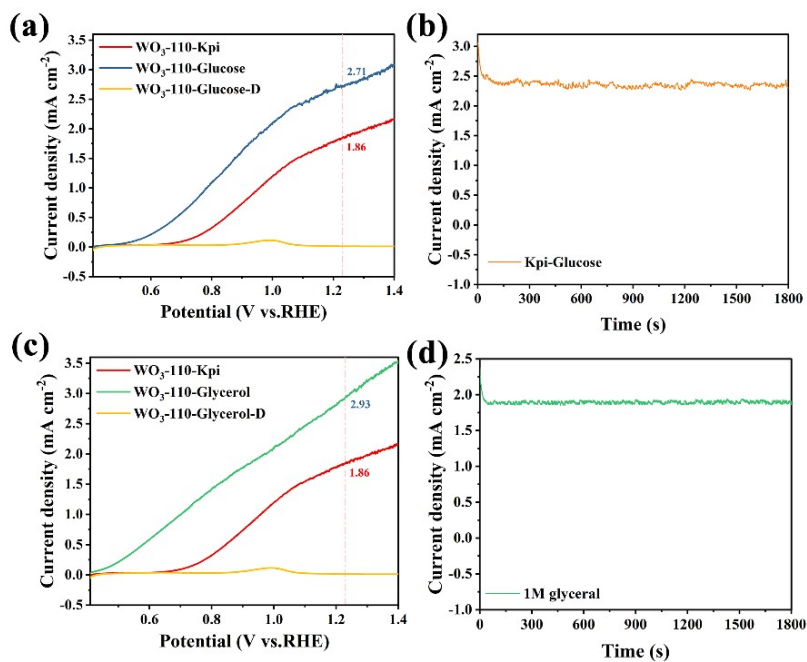


Fig. S12. Electrochemical Testing of h-WO₃-110 in 0.2 M KPi Solution with 0.2 M Glucose and 1 M Glycerol: (a) LSV Curves and (b) i-t Measurements at 1.0 V vs. RHE for Glucose and (c) LSV and (d) i-t at 1.23 V vs. RHE for Glycerol

Notes and references

1. G. Kresse and J. Furthmüller, *Computational Materials Science*, 1996, 6, 15-50.
2. Kresse and Furthmuller, *Physical review. B, Condensed matter*, 1996, 54, 11169-11186.
3. S. Grimme, S. Ehrlich and L. Goerigk, *Journal of Computational Chemistry*, 2011, 32, 1456-1465.
4. P. Guo, B. Tian, J. Liang, X. Yang, G. Tang, Q. Li, Q. Liu, K. Zheng, X. Chen and W. Wu, *Advanced Materials*, 2023, 35, 2304420.
5. C. Jiang, Y. Li, S. Wang, Z. Zhang and Z. Tang, *Electrochimica Acta*, 2018, 278, 290-301.
6. Y. Nukui, N. Srinivasan, S. Shoji, D. Atarashi, E. Sakai and M. Miyauchi, *Chemical Physics Letters*, 2015, 635, 306-311.
7. A. Gomis-Berenguer, J. Iniesta, D. J. Fermín and C. O. Ania, *C*, 2018, 4, 45.
8. L. Li, J. Li, B.-H. Kim and J. Huang, *RSC advances*, 2024, 14, 2080-2087.
9. H. Wu, Q. Liu, L. Zhang, Y. Tang, G. Wang and G. Mao, *ACS Applied Energy Materials*, 2021, 4, 12508-12514.
10. S. S. Kalanur, Y.-G. Noh and H. Seo, *Applied Surface Science*, 2020, 509, 145253.
11. Y. Li, Z. Tang, J. Zhang and Z. Zhang, *Journal of Alloys and Compounds*, 2017, 708, 358-366.
12. A. Hammad, H. M. El-Bery, A. El-Shazly and M. Elkady, *International Journal of Electrochemical Science*, 2018, 13, 362-372.
13. J. Jun, S. Ju, S. Moon, S. Son, D. Huh, Y. Liu, K. Kim and H. Lee, *Nanotechnology*, 2020, 31, 204003.
14. I. Khan, A. Abdalla and A. Qurashi, *international journal of hydrogen energy*, 2017, 42, 3431-3439.
15. M. M. Mohamed, T. M. Salama, M. Hegazy, R. M. Abou Shahba and S. Mohamed, *international journal of hydrogen energy*, 2019, 44, 4724-4736.
16. J. Zhang, Z. Liu and Z. Liu, *ACS applied materials & interfaces*, 2016, 8, 9684-9691.
17. S. Bai, Y. Fang, Y. Zhao, Y. Feng, R. Luo, D. Li and A. Chen, *Journal of Colloid and Interface Science*, 2023, 646, 745-752.
18. S. S. Kalanur and H. Seo, *Journal of Alloys and Compounds*, 2019, 785, 1097-1105.
19. M. Yang, H. He, J. Du, H. Peng, G. Ke and Y. Zhou, *The Journal of Physical Chemistry Letters*, 2019, 10, 6159-6165.